Journal of Nuclear Materials 484 (2017) 332–338

Contents lists available at ScienceDirect

Journal of Nuclear Materials

journal homepage: www.elsevier.com/locate/jnucmat

The effect of fission-energy Xe ion irradiation on the structural integrity and dissolution of the CeO_2 matrix

A.J. Popel [a, b, *], S. Le Solliec [a], G.I. Lampronti [a], J. Day [a], P.K. Petrov [c], I. Farnan [a]

[a] Department of Earth Sciences, University of Cambridge, Downing Street, Cambridge, CB2 3EQ, United Kingdom
[b] Department of Materials, Imperial College London, London, SW7 2AZ, United Kingdom
[c] Department of Materials and London Centre for Nanotechnology, Imperial College London, London, SW7 2AZ, United Kingdom

HIGHLIGHTS

- Ion irradiation induced microstructural rearrangements in CeO_2 thin films.
- Ion irradiation reduced aqueous durability of bulk and thin film CeO_2 samples.
- Secondary phases observed from dissolution of irradiated CeO_2 films in di-water.

ARTICLE INFO

Article history:
Received 14 July 2016
Received in revised form
6 September 2016
Accepted 26 October 2016
Available online 5 November 2016

Keywords:
CeO_2
Thin films
Ion irradiation
Radiation damage
Dissolution
Secondary phases

ABSTRACT

This work considers the effect of fission fragment damage on the structural integrity and dissolution of the CeO_2 matrix in water, as a simulant for the UO_2 matrix of spent nuclear fuel. For this purpose, thin films of CeO_2 on Si substrates were produced and irradiated by 92 MeV $^{129}Xe^{23+}$ ions to a fluence of 4.8×10^{15} ions/cm^2 to simulate fission damage that occurs within nuclear fuels along with bulk CeO_2 samples. The irradiated and unirradiated samples were characterised and a static batch dissolution experiment was conducted to study the effect of the induced irradiation damage on dissolution of the CeO_2 matrix. Complex restructuring took place in the irradiated films and the irradiated samples showed an increase in the amount of dissolved cerium, as compared to the corresponding unirradiated samples. Secondary phases were also observed on the surface of the irradiated CeO_2 films after the dissolution experiment.

1. Introduction

Cerium dioxide, CeO_2, is widely used as a non-radioactive structural analogue to UO_2 to study its dissolution [1–9] and the effect of radiation damage on chemical [10–13] and structural [14–22] stability. This material is also proposed as a possible component in inert matrix fuels or as part of high-level nuclear waste forms.

The use of CeO_2 is justified by the facts that it has the same Fm-3m fluorite type structure with a similar lattice parameter and cation radius as to UO_2 (Table 1) and is considered to be the most appropriate inactive analogue which can serve to gain experience to further work on UO_2.

However, there are important differences that should be remembered. Uranium is an actinide and has six valence electrons, whereas Ce is a lanthanide and has only four valence electrons. Although, there are some similarities in chemical behaviour between actinides and lanthanides, there are no ideal chemical analogues among lanthanides for Th, Pa, U, Pu and Np [27]. Therefore, it is reasonable to expect that chemical behaviour of UO_2 and CeO_2 will be different. The surface of uranium dioxide tends to oxidise in air to UO_{2+x} ($x \leq 1$) [28], implying that some of U^{4+} converts to U^{5+} and U^{6+}. In contrast, in CeO_2 under air atmosphere trace amount of Ce^{3+} tends to be present [1], leading to a CeO_{2-x} composition. Unfortunately, the literature review did not reveal any information on dissolution mechanism of CeO_2 in water, but it is widely accepted that CeO_2 dissolves via reduction of Ce^{4+} to Ce^{3+} [48] under air atmosphere, whereas UO_2 dissolves via oxidation of U^{4+} to U^{6+} [29,30]. Work by Ohno et al. [13], Iwase et al. [12] and Kumar

* Corresponding author. Department of Earth Sciences, University of Cambridge, Downing Street, Cambridge, CB2 3EQ, United Kingdom.
E-mail address: apopel@cantab.net (A.J. Popel).

http://dx.doi.org/10.1016/j.jnucmat.2016.10.046

Table 1
Summary of lattice type, lattice parameter and cation radii for UO_2 and CeO_2.

Parameter	UO_2	CeO_2
Lattice type [23]	Fm-3m fluorite structure	Fm-3m fluorite structure
Lattice parameter (Å)	5.469 [24]	5.411 [25]
Crystal cation radius, r_{cr} (Å) [26]	1.14	1.11

et al. [10] showed that ion irradiation of CeO_2 results in an increased proportion of Ce^{3+} ions, leading to CeO_{2-x}, whereas modelling work by Kinoshita et al. [11] showed that the fission tracks in UO_2 can cause several meta-stable configurations for hyper-stoichiometric defect structures of UO_{2+x}. In addition, work by Sonoda et al. [31] showed that the diameter of ion tracks in UO_2 is much less sensitive to the electronic stopping values than in CeO_2, which indicates that UO_2 has a higher kinetic recovery of the radiation damage than CeO_2. Weber [32] reported that UO_2 has a better recovery of the radiation damage than CeO_2: it was observed that UO_2 irradiated by alpha particles showed 12% recovery of the lattice parameter compared to 10% recovery for CeO_2 following almost two years of post-irradiation storage at room temperature. In addition, the thermal recovery study showed that complete recovery of the lattice parameter was observed by 500 °C for UO_2 and by 700 °C for CeO_2.

Electrical properties of UO_2 and CeO_2 are also different. Stoichiometric UO_2 is a Mott-Hubbard insulator that converts to a p-type semiconductor UO_{2+x} due to oxygen incorporation during oxidation in air [33]. Close to stoichiometric UO_2 has the electrical conductivity values in the range 10^{-3}–10^{-4} S/cm at room temperature [34]. Stoichiometric CeO_2 is a dielectric [35] and tends to convert into CeO_{2-x} in air that is an oxygen deficient n-type semiconductor [36]. Polycrystalline thin film CeO_2 with close to stoichiometric ratio of Ce to O has the electrical conductivity values ~10^{-10} S/cm at room temperature [37].

All these differences question the suitability of using CeO_2 as an UO_2 analogue. To explore this subject further, experimental work with CeO_2 samples was conducted and the obtained results were compared with the similar work on UO_2 samples by Matzke [38]. Matzke [38] considered the effect of radiation damage on dissolution of the UO_2 matrix in water by irradiating UO_2 and UO_2-based simfuel samples with Kr and Rb ions of 40 and 45 keV energy, respectively, to induce radiation damage. This experiment showed that the leach rate of the irradiated samples increased by more than an order of magnitude.

In the current study, we produced thin films of CeO_2 on Si substrates and irradiated with 92 MeV $^{129}Xe^{23+}$ ions to a fluence of 4.8×10^{15} ions/cm^2 along with bulk CeO_2 samples. The irradiated and as-produced films were analysed for comparison using SEM (Scanning Electron Microscopy) and XPS (X-ray Photoelectron Spectroscopy) techniques. The results obtained from the XPS study will be published elsewhere. XRD (X-ray Diffraction) and EPMA (Electron Probe Microanalysis) techniques were used to assess the quality of the as-produced and as-supplied samples. A static batch dissolution experiment was conducted under an air atmosphere. Cerium concentration in the levied solutions was measured using ICP-MS (Inductively Coupled Plasma Mass Spectrometry). The samples after the dissolution experiment were characterised using SEM techniques.

2. Experimental details

2.1. Sample production

The bulk samples of CeO_2 were obtained from Sigma-Aldrich in the form of fused pieces 3–6 mm in size and 99.9% purity on trace metal basis, as claimed by the supplier.

The CeO_2 thin films were grown by pulsed laser deposition (PLD) in a Neocera PLD system with a Lambda Physik KrF laser ($\lambda = 248$ nm) with pulse duration of 50 ns on three (001) oriented p-doped Si substrates with dimensions $10 \times 10 \times 0.5$ mm, secured by silver paste onto the stainless-steel resistive heater at Imperial College London. The target for the PLD system was in-house made from CeO_2 powder (Sigma Aldrich, 99.9% purity, < 5 μm grain size). X-ray diffraction was used to confirm that there was no change in structure from powder to pellet, both presenting a unit cell size a of 5.41 Å. Thin films were deposited from 20 mm diameter stoichometric CeO_2 target in an oxygen pressure of 100 mTorr. The substrate temperature ($T_s = 800$ K) during deposition was controlled using a thermocouple embedded in the heater. The energy density of the laser spot (2×10 mm^2) was 1.5 J/cm^2. From the sample thickness measured using a Dektak 11A, the film growth rate was estimated to be approximately 0.05 nm/pulse. The total number of pulses was 5000 with a repetition rate of 8 Hz. Once the ablation was over, the samples were then cooled down at a rate of 10 °C/min in an oxygen rich environment (760 Torr). The intention was to produce single crystal CeO_2 films in the (111) orientation to utilise the advantages that these samples can offer: idealised simplified system with one crystallographic orientation without grain boundaries and flat surface.

The thin films of CeO_2 were nominally of the same thickness, as they were deposited by the same number of laser pulses, the three samples produced had different colours. This is an indication that the thin films may have had different thicknesses [49].

2.2. Sample irradiation

To simulate the damage produced by fission fragments in nuclear fuel, the samples were irradiated with 92 MeV energy $^{129}Xe^{23+}$ ions to a fluence of 4.8×10^{15} ions/cm^2 on the IRRSUD beamline at the GANIL accelerator, Caen, France [50]. The beamline base vacuum was 6×10^{-7} mbar during the irradiation. The flux was kept at ca. 1.3×10^{10} ions/(cm^2 s) which caused heating of the samples to a temperature not exceeding 150 °C. The temporal structure of the ion beam was 1 ns ion pulse every 100 ns and the beam was swept across the surface of the samples with a frequency of 400 Hz in the horizontal and 4 Hz in the vertical direction to ensure homogenous irradiation. The samples were allowed to cool down to ambient temperature (~19 °C) before the beamline was brought to atmospheric pressure using nitrogen gas to minimise surface oxidation of the samples.

According to the SRIM-2013.00 software [39], the expected nuclear and electronic stopping, dE/dx, for 92 MeV Xe ions in CeO_2 is 0.2 and 20.9 keV/nm, respectively, and the projected ion range is ~7.5 μm. A CeO_2 density value of 7.13 g/cm^3, provided by Sigma-Aldrich for the bulk samples, was assumed in the SRIM calculation. The SRIM results indicate that the Xe ions completely penetrate the CeO_2 thin films (250 nm max) and the electronic stopping regime dominates the dissipation of ion energy throughout the entire film. The Xe ions stop in the substrate at a depth of ~13.5 μm beneath the sample's surface.

2.3. Sample characterisation

The orientation of the as-produced thin film samples was analysed using PANalytical X'Pert MRD diffractometer with X'Celerator detector.

A bulk sample of the as-supplied CeO_2 was powdered using mortar and pestle and analysed in Bragg-Brentano geometry on a D8 Bruker diffractometer equipped with a primary Ge monochromator for Cu Kα1 and a Sol-X solid state detector to verify identity of the sample and check for other phases. In addition, the composition of two bulk samples was examined using a Cameca SX-100 electron microprobe analyser. Prior to the analysis, the samples were embedded in a resin, polished and carbon coated to ensure conductivity for the analysis. Calibration of the equipment was performed using a set of rare earth elements.

Surface morphology of the CeO_2 samples was studied using JEOL 820 SEM. No conductive coating was used for the thin film samples to preserve the surface for subsequent studies. A bulk sample of CeO_2 was gold-coated to improve surface conductivity. In addition, uncoated irradiated (to preserve the surface for further studies) and unirradiated bulk samples were studied on a FEI Quanta650F instrument operating at 2 kV with spot size 1 under high vacuum.

2.4. Dissolution experiment

Dissolution experiments were conducted to assess the effect of the xenon ion irradiation on the CeO_2 matrix dissolution in water. Table 2 summarises the set of CeO_2 samples used for the dissolution study.

First of all, the samples listed in Table 2 were rinsed with deionised water and pre-washed by placing into plastic bottles with ~10 ml of deionised water for a day. The Milli-Q water (18.2 MΩ/cm) was used throughout this experiment. The aim of this approach was to remove fine CeO_2 particles on the surface of the samples that were observed in SEM (Fig. 2a), as they can affect Ce concentration measurements. After a day of pre-washing, the pre-washed samples were rinsed with the deionised water and allowed to dry before they were placed into the leaching vessels filled with 4 ml of the deionised water. The leaching vessels consisted of a stainless steel casing with a tight lid on the thread and a PTFE (polytetrafluoroethylene) liner. In addition, two blank leaching vessels were prepared for reference purposes. The leaching vessels were placed in a heater set to 90 °C. The elevated temperature was used to facilitate dissolution, as it is known that CeO_2 is highly insoluble in water. Static replenishment leaching tests were performed where ~1.5 ml of the solution sample was taken at a certain time from each leaching vessel using a syringe with a 0.45 μm filter and ~1.5 ml of the fresh deionised water was replenished in each vessel to maintain the volume of solutions constant thought the experiment. The solution samples were taken over the duration of 27 days at an ambient temperature of 20–25 °C.

To ensure that there is enough solution volume for the ICP-MS analysis, 1 ml of the deionised water was added into each vial, and the solutions were acidified using 45 μl of 15.5 M nitric acid. The presented Ce concentrations (in Fig. 5 and Fig. 6) were corrected for the acid and water additions and represent ^{140}Ce concentration (88.48% natural abundance) [51] before the dilutions.

The leaching of samples Ce-SLS-1 and Ce-SLS-2 was stopped after 25 days. These two samples were selected to examine the precipitation of Ce on the walls of the liners. These liners were emptied, rinsed with the deionised water and gently wiped. Then, 4.5 ml of 1 M nitric acid were added in each liner and the leaching vessels were placed in a heater set to 90 °C for three days. The samples for ICP-MS analysis from these acidic solutions were prepared by adding 0.66 ml of the solution to 2.5 ml of the deionised water to keep the same acidity between all the samples to minimise any bias during the subsequent analysis.

The extracted solutions were analysed on a Perkin Elmer SCIEX Elan DRC II quadrupole ICP-MS. The calibration standards for Ce and other rare earth elements (blank, 0.1, 0.25, 1, 10, 100 ppb (mass basis)) were prepared as an external calibration using serial dilutions of a mixed rare earth element standard (CPI International, California, USA) and also a multi element standard (SPS-SW2, LGC Standards, UK) in high purity 1 vol% HNO_3 (quartz distilled in house). The regular analysis of the 0.25 ppb Ce quality control standard showed a maximum error in Ce concentration of 7%. The measured Ce concentration for the blank runs was in the range 1×10^{-11} to 4×10^{-11} mol/l. Hence, the measurement error of 7% or $\pm 4 \times 10^{-11}$ mol/l, whichever is greater, should be applied to the obtained Ce concentration values. The error bars are not plotted on the dissolution graphs below for the sake of clarity as their sizes do not affect the observed trends.

Following dissolution, the irradiated and unirradiated thin film samples were analysed using a JEOL 820 SEM.

Table 2
Summary of the CeO_2 samples used for the dissolution study.

Sample name	Sample description
Ce-AP1	unirradiated thin film of CeO_2
Ce-AP2*	Xe irradiated thin film of CeO_2
Ce-AP3*	Xe irradiated thin film of CeO_2
Ce-SLS1	unirradiated bulk CeO_2
Ce-SLS2	unirradiated bulk CeO_2
Ce-SLS3	unirradiated bulk CeO_2
Ce-AP5*	Xe irradiated bulk CeO_2

3. Results

3.1. Sample characterisation

It is expected that the produced films have different thickness as they have different colours [49]. Film thickness was not measured due to technical limitations but the target film thickness was 250 nm.

Crystallographic orientation of the as-produced thin films was examined by XRD (Fig. 1). All three samples showed a 111 reflection from the CeO_2 film and a 400 reflection from Si substrate. In addition, sample Ce-AP2 showed a weak 200 CeO_2 reflection, two unidentified reflections at 36.9° and 38.0° and a strong 222 CeO_2 reflection. We suggest that samples Ce-AP1 and Ce-AP3 are single

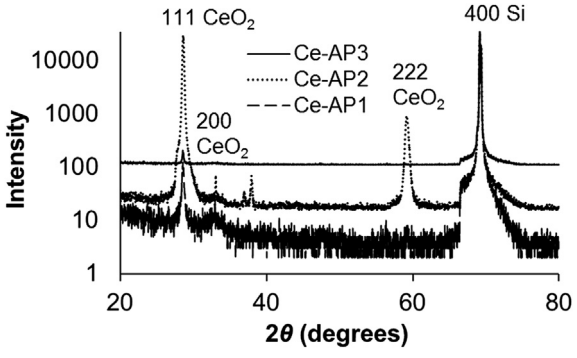

Fig. 1. XRD results for the as-produced CeO_2 thin film samples. The trace for sample Ce-AP1 is at the bottom, for sample Ce-AP2 is in the middle and for sample Ce-AP3 it is at the top. The peaks at 36.9° and 38.0° for sample Ce-AP2 are not identified. XRD intensity for samples Ce-AP2 and Ce-AP3 is shifted upwards for clarity.

crystals, although further work is needed to prove this (for example, XRD in-plane φ scans as described in the work by Strehle et al. [23]), and sample Ce-AP2 is preferentially oriented in (111) with (001) domains also present. The unidentified reflections might result from a Si–Ce or Si–Ce–O phase formed at the film-substrate interface during the sample growth stage. Edmondson et al. [15] reported that there are six different phases of cerium silicides [40,41]: Ce_5Si_3, Ce_3Si_2, Ce_5Si_4, CeSi, Ce_3Si_5 and $CeSi_2$; and various oxides including $CeSiO_3$ [42], $Ce_2Si_2O_7$ [43] and $CeSiO_4$ [44].

Electron probe microanalysis was performed for two bulk CeO_2 samples to assess purity of the samples. The analysis indicated that Gd impurity was present at ~6 wt% and there were some traces of Sm, Eu and La. However, X-ray diffraction of a powdered bulk CeO_2 sample produced a diffraction pattern identical to the reference one and no Gd containing phase was observed, since Gd is soluble in CeO_2 up to ~36 wt% and does not change much the lattice parameter especially for low loadings [45].

The surface topography of the samples was studied using SEM. The fused pellet exhibited cracks at the grain boundaries, which indicate incomplete sintering or crack formation during the cooling stage (not shown), and sub-micron particles present at the surface (Fig. 2a). The ion irradiation caused formation of a wavy pattern on the surface of the irradiated bulk samples (Fig. 2b).

The surface of unirradiated thin film sample Ce-AP1 is smooth and contains occasional 0.5–1 μm pores (not shown). Thin film sample Ce-AP2* developed the regular circular holes with a diameter 6–7 μm (Fig. 3a) along with the larger formations (Fig. 3b) with a dimension ~15 μm as a result of the ion irradiation. We are inclined to suggest that the larger formations form by coalescence of the smaller holes as evidenced by the arched edges of the larger formations. Some of the holes tend to have islands of CeO_2 material in the central region of the hole with dimensions ≤1 μm. Near the edges of the holes and around the islands much smaller (≤0.1 μm) circular fragments of CeO_2 material were observed.

The high fluence irradiation of thin film sample Ce-AP3* caused disintegration of the film into discrete fragments with circular and elongated shapes with the size range of 0.2–1.5 μm for the circular fragments and 2–6 μm for the elongated fragments (Fig. 4). Much smaller circular fragments (≤0.1 μm) around the larger fragments were observed again and the Si substrate showed some signs of the irradiation damage in the form of holes (not shown).

3.2. Dissolution results

Fig. 5 presents a plot of cerium concentration versus time for the thin film samples of CeO_2. The irradiated thin films showed higher Ce concentration in water than the unirradiated thin film – 180 times higher for irradiated sample Ce-AP2* and 28 times higher for irradiated sample Ce-AP3*, as compared to unirradiated sample Ce-AP1 on the 27th day of leaching. This indicates that the ion irradiation increased CeO_2 dissolution in water. In addition, irradiated sample Ce-AP2* showed higher concentration of Ce (~6 times) than irradiated sample Ce-AP3*, as measured on the last day of leaching. The reason for this arises, more likely, from different thickness of the films.

The presence of a maximum in the dissolution curves indicates that precipitation of cerium containing secondary phases is likely to take place – dissolution-precipitation behaviour is expected. The concentration values of Ce in the pre-wash solutions were 19, 1.2 and 0.7 times the values after one day of leaching for thin film CeO_2 samples Ce-AP1, Ce-AP2* and Ce-AP3*, respectively. Gadolinium ions were also detected in solutions (up to 2.5×10^{-9} mol/l for sample Ce-AP2*), indicating that the stock CeO_2 powder used for production of the thin films had also gadolinium as an impurity.

Fig. 6 presents a plot of cerium concentration as a function of time for the bulk samples of CeO_2. Again, the irradiated bulk sample showed higher Ce concentration in water than the unirradiated bulk samples – 14 times higher for irradiated sample Ce-AP5*, as compared to unirradiated sample Ce-SLS3 on the 27th day of leaching. Again, this indicates that the Xe ion irradiation increased CeO_2 dissolution in water. Irradiated bulk sample Ce-AP5* showed a dissolution curve with different gradients that were positive for all days of leaching. This indicates that the initial dissolution mechanism was altered and that equilibrium was not attained in the system. The dissolution mechanism can be altered by secondary phases precipitating at the surface of the sample and limiting the access of the sample's surface to water or it might be the case that the next stage of the dissolution is dominated by the dissolution of these secondary phases.

The measured Ce concentration values for the unirradiated bulk CeO_2 samples were within the experimental error of each other ($\pm 4 \times 10^{-11}$ mol/l error is used in this case) and this makes impossible to comment on the shape of the dissolution curves. The concentration values of Ce in the pre-wash solutions were 11–55 times higher than the values after one day of leaching for the irradiated and unirradiated CeO_2 bulk samples. This likely indicates that the surface of the bulk samples had loose cerium containing fine particles, which is consistent with the SEM study (Fig. 2a). The Ce concentration values in acid wash solutions were ~200 times higher than the values on the last day of leaching for CeO_2 bulk

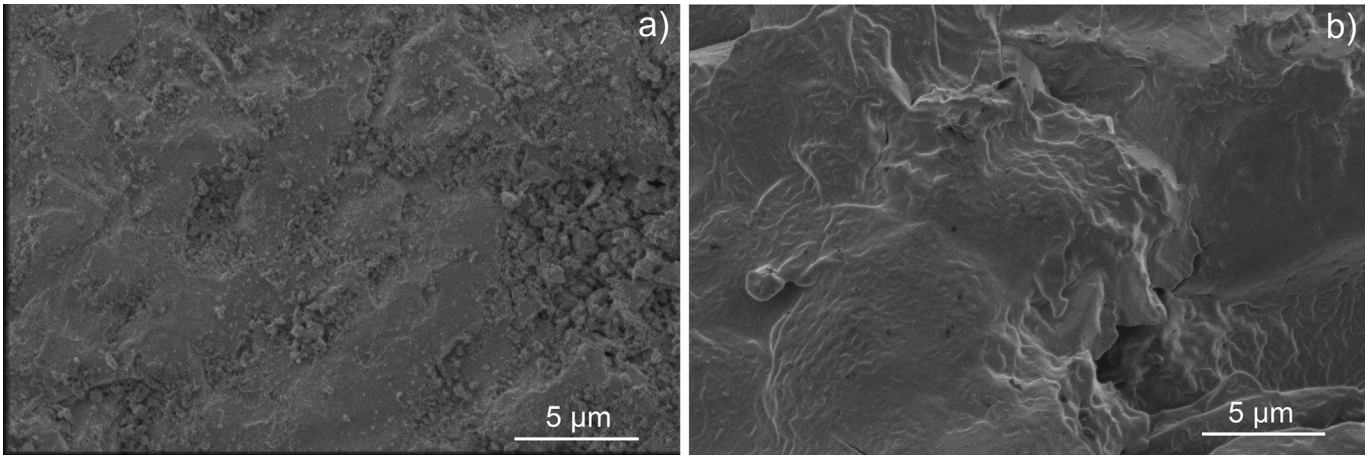

Fig. 2. Secondary electron SEM images of the surface topography of: a) an unirradiated bulk sample of CeO_2, b) a $^{129}Xe^{23+}$ ion irradiated bulk sample of CeO_2.

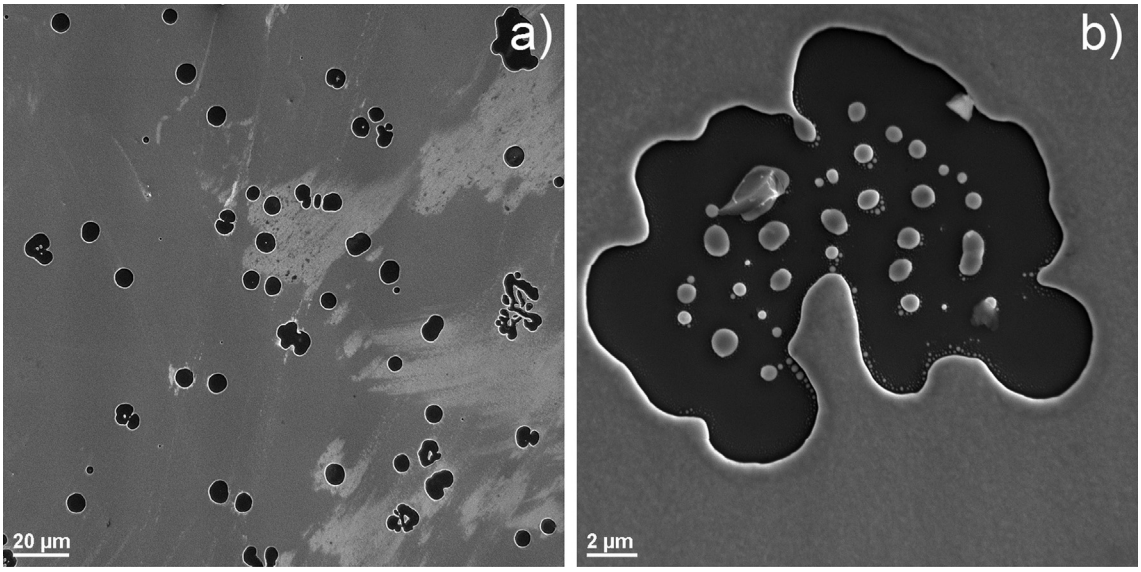

Fig. 3. Secondary electron SEM images of the surface topography of $^{129}Xe^{23+}$ ion irradiated thin film sample Ce-AP2*: a) low magnification, b) high magnification.

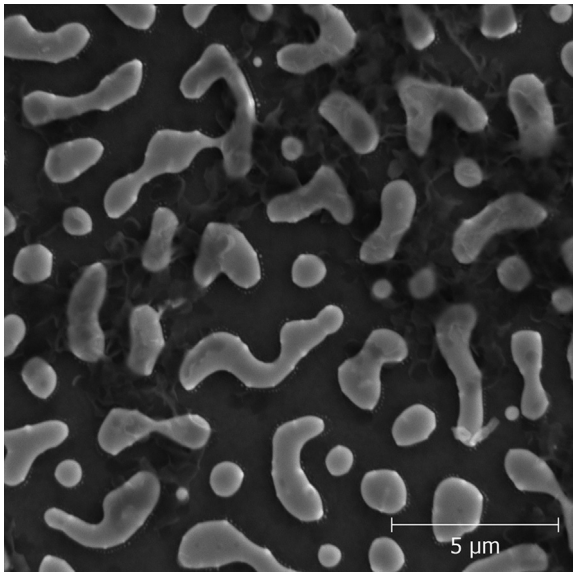

Fig. 4. A secondary electron SEM image of the surface topography of $^{129}Xe^{23+}$ ion irradiated thin film sample Ce-AP3*.

samples Ce-SLS1 and Ce-SLS2. Again, gadolinium ions were detected in solutions (~10^{-11} mol/l) supporting the electron microprobe results.

The pH values of the solutions were measured at the end of leaching once the samples were removed and were in the range 5.1–5.6. The pH value of the deionised water used for the leaching was slightly acidic (pH = 5.7), more likely, due to absorption of atmospheric CO_2. Hence, dissolution of CeO_2 resulted in a decrease of the pH values, as compared to the value of the deionised water. The most pronounced change in the pH value was observed for irradiated bulk sample Ce-AP5* (pH = 5.1), as compared to the value of the deionised water.

3.3. Post-dissolution results

Unirradiated thin film sample Ce-AP1 after the dissolution

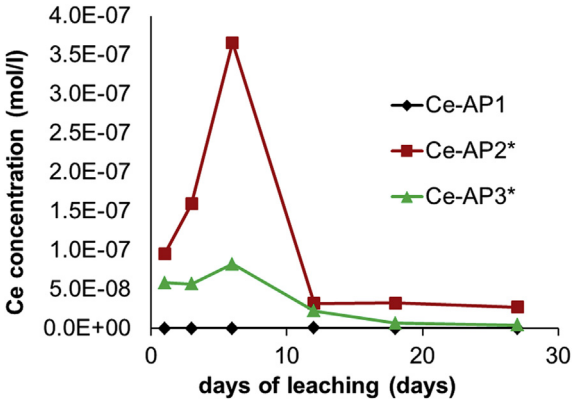

Fig. 5. A plot of Ce concentration as a function of leaching time for the thin film samples of CeO_2. The solid lines are only added to guide the eye.

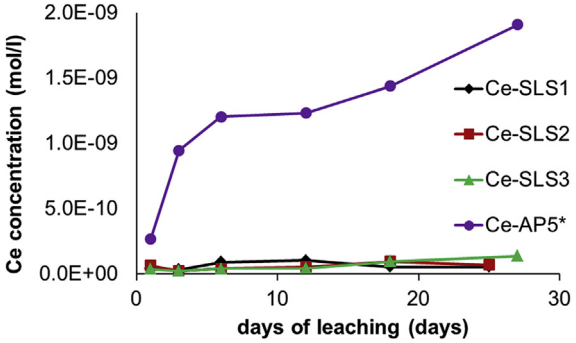

Fig. 6. A plot of Ce concentration as a function of leaching time for the bulk samples of CeO_2. The solid lines are only added to guide the eye.

experiment did not show any noticeable surface alternations, as indicated by SEM study (not shown). SEM image of the surface of irradiated thin film sample Ce-AP2* after the dissolution experiment (Fig. 7) suggests that the holes, which were observed before the leaching experiment (Fig. 3), increased in size to ~30 μm and a secondary phase precipitated in the middle of the holes and

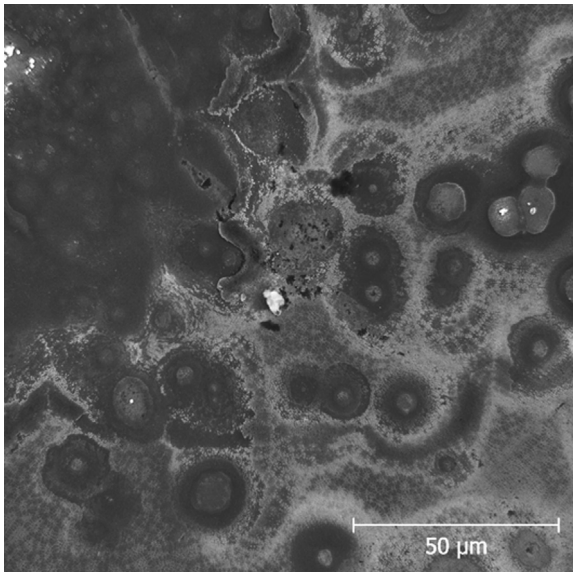

Fig. 7. A secondary electron SEM image of the surface topography of $^{129}Xe^{23+}$ irradiated thin film sample Ce-AP2* after the dissolution experiment. Secondary phases appear in white.

between them.

The surface topography of irradiated thin film sample Ce-AP3* after the dissolution experiment did not show any significant changes (Fig. 8). The small circular satellites around the larger features, observed in Fig. 4, disappeared, more likely, as a result of dissolution. Instead, rod-shape particles with a length of 0.2 μm and a width of 0.05 μm appeared attributed to cerium secondary phases.

4. Discussion

The radiation damage induced by Xe ion irradiation resulted in the increased cerium concentration values as was shown by the

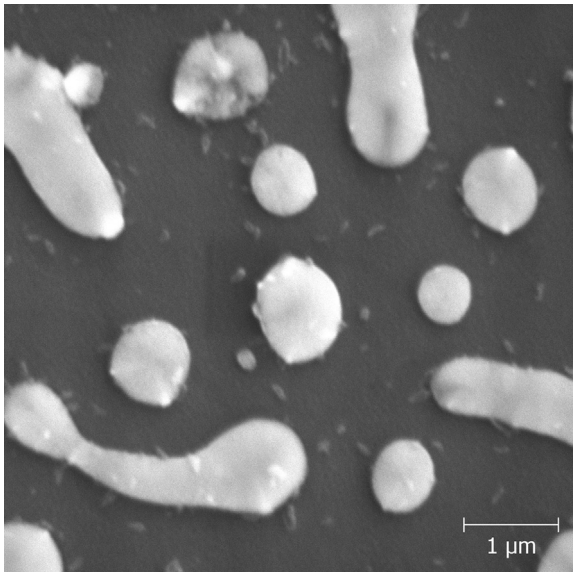

Fig. 8. A secondary electron SEM image of the surface topography of $^{129}Xe^{23+}$ irradiated thin film sample Ce-AP3* after the dissolution experiment. Rod-shape particles around the larger features can be seen.

CeO_2 thin film and bulk samples. The effect is most likely caused by an increased proportion of Ce^{+3} ions in the CeO_2 matrix due to the Xe ion irradiation [10,12,13]. Ce^{3+} can be more easily removed from the CeO_{2-x} surface than Ce^{4+}. In addition, the expected increase in Ce^{3+} fraction should result in hypo-stoichiometry, CeO_{2-x}, to maintain the charge balance [10]. The electrical conductivity of CeO_{2-x} tends to increase with increase in x up to $x = 0.1$ [46]. Hence, the dissolution rate is also expected to increase [30]. However, the overall effect of the radiation damage on the electrical conductivity in CeO_2 can be more complex, as was the case for UO_2 (Fig. 2 in Ref. [34]). Hence, the exact effect of the radiation damage on the electrical conductivity in CeO_2 remains unknown. Incorporation of Si from the silicon substrate into the CeO_2 lattice to form a substitutional solid solution, as a result of the irradiation induced mixing, is unlikely, as a Si^{4+} ion is half the size of a Ce^{4+} ion [26]. Hence, stabilisation or distortion of the CeO_2 lattice by the substrate Si is not expected.

The dissolution data from the thin films should be treated with some caution. The difference in the film thickness might imply that thinner samples have more Ce^{3+} on the surface that is more soluble than Ce^{4+}. Hence, the effect of the radiation damage enhanced dissolution might interfere with the enhanced dissolution caused by a higher proportion of Ce^{3+} ions due to smaller film thickness.

Horlait et al. [5] showed that incorporation of Gd into CeO_2 results in an increased dissolution rate of $Ce_{1-x}Gd_xO_{2-x/2}$ in acidic solution attributed to weakening of the crystal lattice due to oxygen vacancies, formed to ensure charge balance following Gd^{3+} incorporation. Since the irradiated and unirradiated samples in this work should have the same content of Gd, the presence of gadolinium should not affect the observed trend caused by the ion irradiation.

The pre-wash concentration results show the significance of a more soluble material at the surface of the samples that dissolves in the first instance. An initial burst of leaching is a very common phenomenon that is observed for many materials, although the reasons for this (surface defects, surface oxidation/reduction?) are still unclear.

The observed decrease of the pH values as a result of the CeO_2 dissolution, which correlates with the extent of dissolution, can be potentially explained in terms of the hydrolysis of Ce^{4+} and Ce^{3+} as suggested by Hayes at al [47].:

$$Ce^{4+} + iH_2O \rightarrow Ce(OH)_i^{4-i} + iH^+ \quad [1]$$

$$Ce^{3+} + nH_2O \rightarrow Ce(OH)_n^{3-n} + nH^+ \quad [2]$$

The acid leaching of the vessels, in which CeO_2 dissolution took place, indicates that significant precipitation of the secondary Ce containing phases was taking place on the walls of the liners and on the surface of the samples. The extensive secondary phase precipitation in this dissolution experiment is facilitated by two mechanisms: 1) the intrinsic dissolution-precipitation behaviour of CeO_2 in water that is indicated by the presence of a maximum in the dissolution curves; 2) the cooling of solution from 90 °C to an ambient temperature of ~20–25 °C that might result in reaching the saturation concentration of dissolved cerium. Further work is required to identify these secondary phases.

The observed microstructural response in the CeO_2 thin films to the ion irradiation is a microscale cumulative effect of the irradiation damage. The difference in microstructural response of thin film Ce-AP2 and Ce-AP3, more likely, can be attributed to different thickness of the films. The irradiated CeO_2 thin films developed a different microstructure to that observed for UO_2 thin films on LSAT (Lanthanum Strontium Aluminium Tantalum oxide) substrates irradiated under the same conditions in Ref. [50].

Despite the differences between CeO_2 and UO_2 outlined in the introduction section, the observed dissolution response for the irradiated CeO_2 thin film and bulk samples is in qualitative agreement with the work by Matzke [38], where it was observed that the leach rate of the ion irradiated UO_2 and UO_2-based simfuel samples increased compared the corresponding unirradiated samples. For a better comparison, thin films of CeO_2 and UO_2 could be produced with the same thickness on the same substrates and irradiated under the same conditions along with the polished bulk samples and subsequently characterised to reveal any differences in structural and chemical responses to the irradiation damage.

5. Conclusions

It was observed that the high energy, high fluence ion irradiation resulted in significant microstructural rearrangements of the CeO_2 thin films. It was also suggested that the microstructural rearrangement due to an ion irradiation depends on thickness of the film being irradiated.

An increase in the measured Ce concentration values for the irradiated bulk and thin film CeO_2 samples was observed, as compared to the unirradiated samples. This observation is in qualitative agreement with the work by Matzke [38], where an increase in the leach rate of the UO_2 matrix was observed as a result of radiation damage by ion irradiations.

Secondary phases were observed on the surface of the irradiated thin film samples after the dissolution experiment.

Supporting data

Supporting data will be available in A.J. Popel's PhD thesis (University of Cambridge) published online.

Acknowledgments

The irradiation experiment was performed at the Grand Accélérateur National d'Ions Lourds (GANIL) Caen, France, and supported by the French Network EMIR. The support in planning and execution of the experiment by the CIMAP-CIRIL and the GANIL staff, especially, I. Monnet, C. Grygiel, T. Madi and F. Durantel is much appreciated.

Thanks are given to I. Buisman and M. Walker from the Department of Earth Sciences, University of Cambridge for help in conducting electron probe microanalysis and polishing the samples, respectively.

A.J. Popel acknowledges funding from the UK EPSRC (grant EP/I036400/1 and EP/L018616/1) and Radioactive Waste Management Ltd (formerly the Radioactive Waste Management Directorate of the UK Nuclear Decommissioning Authority, contract NPO004411A-EPS02).

References

[1] M.C. Stennett, C.L. Corkhill, L.A. Marshall, N.C. Hyatt, J. Nucl. Mater. 432 (2013) 182–188.
[2] L. Claparede, N. Clavier, N. Dacheux, P. Moisy, R. Podor, J. Ravaux, Inorg. Chem. 50 (2011) 9059–9072.
[3] M. Virot, T. Chave, D. Horlait, N. Clavier, N. Dacheux, J. Ravaux, S.I. Nikitenko, J. Mater. Chem. 22 (2012) 14734–14740.
[4] L. Claparede, N. Clavier, N. Dacheux, A. Mesbah, J. Martinez, S. Szenknect, P. Moisy, Inorg. Chem. 50 (2011) 11702–11714.
[5] D. Horlait, N. Clavier, S. Szenknect, N. Dacheux, V. Dubois, Inorg. Chem. 51 (2012) 3868–3878.
[6] C.L. Corkhill, D.J. Bailey, S.M. Thornber, M.C. Stennett, N.C. Hyatt, Mater. Res. Soc. Symp. Proc. 1518 (2013) 151–156.
[7] C.L. Corkhill, E. Myllykyla, D.J. Bailey, S.M. Thornber, J. Qi, P. Maldonado, M.C. Stennett, A. Hamilton, N.C. Hyatt, ACS Appl. Mater. Interfaces 6 (2014) 12279–12289.
[8] C.L. Corkhill, M.C. Stennett, N.C. Hyatt, Mater. Res. Soc. Symp. Proc. 1744 (2015) 185–190.
[9] C.L. Corkhill, D.J. Bailey, F.Y. Tocino, M.C. Stennett, J.A. Miller, J.L. Provis, K.P. Travis, N.C. Hyatt, ACS Appl. Mater. Interfaces 8 (2016) 10562–10571.
[10] A. Kumar, R. Devanathan, V. Shutthanandan, S.V.N.T. Kuchibhatla, A.S. Karakoti, Y. Yong, S. Thevuthasan, S. Seal, J. Phys. Chem. C 116 (2012) 361–366.
[11] M. Kinoshita, K. Yasunaga, T. Sonoda, A. Iwase, N. Ishikawa, M. Sataka, K. Yasuda, S. Matsumura, H.Y. Geng, T. Ichinomiya, Y. Chen, Y. Kaneta, M. Iwasawa, T. Ohnuma, Y. Nishiura, J. Nakamura, Hj. Matzke, Nucl. Instr. Meth. Phys. Res. B 267 (2009) 960–963.
[12] A. Iwase, H. Ohno, N. Ishikawa, Y. Baba, N. Hirao, T. Sonoda, M. Kinoshita, Nucl. Instr. Meth. Phys. Res. B 267 (2009) 969–972.
[13] H. Ohno, A. Iwase, D. Matsumura, Y. Nishihata, J. Mizuki, N. Ishikawa, Y. Baba, N. Hirao, T. Sonoda, M. Kinoshita, Nucl. Instr. Meth. Phys. Res. B 266 (2008) 3013–3017.
[14] T. Kishino, K. Shimizu, Y. Saitoh, N. Ishikawa, F. Hori, A. Iwase, Nucl. Instr. Meth. Phys. Res. B 314 (2013) 191–194.
[15] P.D. Edmondson, N.P. Young, C.M. Parish, S. Moll, F. Namavar, W.J. Weber, Y. Zhang, T. Mitchell, J. Am. Ceram. Soc. 96 (2013) 1666–1672.
[16] N. Ishikawa, K. Takegahara, Nucl. Instr. Meth. Phys. Res. B 272 (2012) 227–230.
[17] P.D. Edmondson, Y. Zhang, S. Moll, F. Namavar, W.J. Weber, Acta Mater. 60 (2012) 5408–5416.
[18] Y. Tahara, B. Zhu, S. Kosugi, N. Ishikawa, Y. Okamoto, F. Hori, T. Matsui, A. Iwase, Nucl. Instr. Meth. Phys. Res. B 269 (2011) 886–889.
[19] K. Ohhara, N. Ishikawa, S. Sakai, Y. Matsumoto, O. Michikami, Y. Ohta, Nucl. Instr. Meth. Phys. Res. B 267 (2009) 973–975.
[20] T. Sonoda, M. Kinoshita, N. Ishikawa, M. Sataka, Y. Chimi, N. Okubo, A. Iwase, K. Yasunaga, Nucl. Instr. Meth. Phys. Res. B 266 (2008) 2882–2886.
[21] N. Ishikawa, Y. Chimi, O. Michikami, Y. Ohta, K. Ohhara, M. Lang, R. Neumann, Nucl. Instr. Meth. Phys. Res. B 266 (2008) 3033–3036.
[22] T. Sonoda, M. Kinoshita, Y. Chimi, N. Ishikawa, M. Sataka, A. Iwase, Nucl. Instr. Meth. Phys. Res. B 250 (2006) 254–258.
[23] M.M. Strehle, B.J. Heuser, M.S. Elbakhshwan, X. Han, D.J. Gennardo, H.K. Pappas, H. Ju, Thin Solid Films 520 (2012) 5616–5626.
[24] Z. Bao, R. Springell, H.C. Walker, H. Leiste, K. Kuebel, R. Prang, G. Nisbet, S. Langridge, R.C.C. Ward, T. Gouder, R. Caciuffo, G.H. Lander, Phys. Rev. B 88 (2013) 134426.
[25] H.J. Whitfield, D. Roman, A.R. Palmer, J. Inorg. Nucl. Chem. 28 (1966) 2817–2825.
[26] R.D. Shannon, Acta Cryst. A32 (1976).
[27] B.E. Burakov, M.I. Ojovan, W.E. Lee, Crystalline Materials for Actinide Immobilisation, vol. 1, Imperial College Press, 2011, 8, 59.
[28] R.J. McEachern, P. Taylor, J. Nucl. Mater. 254 (1998) 87–121.
[29] D.W. Shoesmith, J. Nucl. Mater. 282 (2000) 1–31.
[30] D.W. Shoesmith, S. Sunder, J. Nucl. Mater. 190 (1992) 20–35.
[31] T. Sonoda, M. Kinoshita, N. Ishikawa, M. Sataka, A. Iwase, K. Yasunaga, Nucl. Instr. Meth. Phys. Res. B 268 (2010) 3277–3281.
[32] W.J. Weber, Radiat. Eff. 83 (1984) 145–156.
[33] H. He, Z. Qin, D.W. Shoesmith, Electrochim. Acta 56 (2010) 53–60.
[34] N. Nakae, T. Koike, T. Kirihara, J. Nucl. Mater. 73 (1978) 217–221.
[35] J. Lappalainen, D. Kek, H.L. Tuller, J. Eur. Ceram. Soc. 24 (2004) 1459–1462.
[36] H.L. Tuller, A.S. Nowick, J. Electrochem. Soc. 126 (1979) 209–217.
[37] D. Kek-Merl, J. Lappalainen, H.L. Tuller, J. Electrochem. Soc. 153 (2006) J15.
[38] Hj. Matzke, J. Nucl. Mater. 190 (1992) 101–106.
[39] J.F. Ziegler, J.P. Biersack, M.D. Ziegler, The Stopping and Range of Ions in Matter, SRIM Co., Chester, Maryland, U.S.A, 2008.
[40] H. Okamoto, J. Phase Equilib. Diffus. 25 (2004) 98–99.
[41] F. Weitzer, J.C. Schuster, J. Bauer, B. Jounel, J. Mater. Sci. 26 (1991) 2076–2080.
[42] F.U. Hillebrecht, M. Ronay, D. Rieger, F.J. Himpsel, Phys. Rev. B 34 (1986) 5377–5380.
[43] R. Barnes, D. Starodub, T. Gustafsson, E. Garfunkel, J. Appl. Phys. 100 (2006) 044103.
[44] J. Schlüter, T. Malcherek, T.A. Husdal, N. Jb, Miner. Abh 186 (2009) 195–200.
[45] D. Horlait, L. Claparède, N. Clavier, S. Szenknect, N. Dacheux, J. Ravaux, R. Podor, Inorg. Chem. 50 (2011) 7150–7161.
[46] R.N. Blumenthal, R.L. Hofmaier, J. Electrochem. Soc. 121 (1974) 126–131.
[47] S.A. Hayes, P. Yu, T.J. O'Keefe, M.J. O'Keefe, J.O. Stoffer, J. Electrochem. Soc. 149 (2002) C623–C630.
[48] T.V. Plakhova, A.Y. Romanchuk, S.N. Yakunin, T. Dumas, S. Demir, S. Wang, S.G. Minasian, D.K. Shuh, T. Tyliszczak, A.A. Shiryaev, A.V. Egorov, V.K. Ivanov, S.N. Kalmykov, J. Phys. Chem. C 120 (2016) 22615–22626.
[49] L.M. Liz-Marzán, Mater. Today 7 (2004) 26–31.
[50] A.J. Popel, V.A. Lebedev, P.G. Martin, A.A. Shiryaev, G.I. Lampronti, R. Springell, S.N. Kalmykov, T.B. Scott, I. Monnet, C. Grygiel, I. Farnan, J. Nucl. Mater. 482 (2016) 210–217.
[51] J.H.L. Voncken, The Rare Earth Elements, Springer International Publishing, 2016, p. 60.